Planetary Nebulae: A Universal Toolbox in the Era of Precision Astrophysics
Proceedings IAU Symposium No. 384, 2025
O. De Marco, A. Zijlstra & R. Szczerba, eds.
doi:10.1017/S1743921324000498

High-Speed Outflows and Dusty Disks during the AGB to PN Transition: The PANORAMA survey

Raghvendra Sahai[1], Javier Alcolea[2], Bruce Balick[3], Eric G. Blackman[4], Valentin Bujarrabal[2], Arancha Castro-Carrizo[5], Orsola De Marco[6], Joel H. Kastner[7], Hyosun Kim[8], Eric Lagadec[9], Chin-Fei Lee[10], Laurence Sabin[11], M. Santander-García[2], Carmen Sánchez Contreras[12], Daniel Tafoya[13], Toshiya Ueta[14], Wouter Vlemmings[13] and Albert Zijlstra[15]

[1]Jet Propulsion Laboratory, Pasadena, CA, USA

[2]Observatorio Astronómico Nacional (IGN/CNIG), MITMA, Spain

[3]Dept. of Astronomy, University of Washington, Seattle, WA 98195-1580, USA

[4]Dept. of Physics & Astronomy, U. Rochester Rochester, NY, 14621, USA

[5]Institut de Radioastronomie Millimétrique, 300 rue de la Piscine, 38406 Saint-Martin-d'Heres, France

[6]School of Mathematical and Physical Sciences, Macquarie University, Sydney, New South Wales, Australia

[7]Rochester Institute of Technology, Rochester, NY 14623 USA

[8]Korea Astronomy and Space Science Institute, 776, Daedeokdae-ro, Yuseong-gu, Daejeon 34055, Republic of Korea

[9]Université Côte d'Azur, CNRS, Boulevard de l'observatoire, CEDEX 4, 06304 Nice, France

[10]Academia Sinica Institute of Astronomy and Astrophysics, No. 1, Sec. 4, Roosevelt Road, Taipei 106, Taiwan

[11]Instituto de Astronomía, Universidad Nacional Autónoma de México, Apdo. Postal 877, C.P. 22860, Ensenada, B.C., México

[12]Centro de Astrobiología (CAB), CSIC-INTA. Postal address: ESAC, Camino Bajo del Castillo s/n, E-28692, Villanueva de la Cañada, Madrid, Spain

[13]Chalmers University of Technology, Onsala Space Observatory, Onsala, Sweden

[14]University of Denver, USA

[15]Jodrell Bank Centre for Astrophysics, Dept. of Physics and Astronomy, University of Manchester, Manchester, UK

Abstract. As AGB stars evolve to planetary nebulae (PNe), the geometry of the ejected mass transforms from nearly spherical to extremely aspherical. The mechanisms governing this transformation are plausibly linked to binarity and the associated production of disks and jets during the transitional (post-AGB) evolutionary stage. We are carrying out an ALMA survey of a representative sample of bipolar/multipolar post-AGB objects to obtain high angular-resolution ($0\farcs1$) observations of the CO(3–2) and 6–5 emission and study the collimated outflows and central disks. We present highlights from our ongoing survey – e.g., the presence of bipolar or multipolar high-velocity outflows, dense toroidal waists, and in one case, a circular ring around the central bipolar nebula. We will use radiative transfer modeling to derive accurate outflow momenta, masses, and mass-loss rates for our sample, thereby constraining different classes of binary PN-shaping models.

Keywords. stars: AGB and post-AGB, stars: mass loss, binaries, planetary nebulae, ISM: jets and outflows, surveys

1. Introduction

Understanding the impact of binary interactions on stellar evolution is a major challenge – these interactions dominate a substantial fraction of stellar phenomenology (Ivanova et al. 2013; Bond et al. 2003; Tylenda et al. 2011), and likely play a major role in the formation of most Planetary Nebulae (PNe), objects that represent the bright end-stages of most stars in the Universe. Such interactions can help explain why, even though the progenitors of PNe – AGB stars and their circumstellar envelopes – are generally slowly-expanding ($V_{exp} \sim$ 5-15 km s^{-1}) round structures, the vast majority of PNe deviate strongly from spherical symmetry, showing a dazzling variety of bipolar, multipolar, and elliptical morphologies (Sahai & Trauger 1998; Ueta et al. 2000; Sahai et al. 2011; Stanghellini et al. 2016). A morphological survey of objects in the evolutionary transition stage between AGB stars and PNe, i.e., pre-planetary nebulae (PPNe), shows a complete lack of round objects (Sahai et al. (2007), hereafter $Setal07$; Siódmiak et al. (2008); Lagadec et al. (2011)). In addition, PPNe also show the presence of fast outflows ($V_{exp} \gtrsim$ 50-100 km s^{-1}), which, when resolved (using interferometric observations), are generally highly-collimated. Dense, dusty, equatorial waists are also frequently found in PPNe and PNe, and recognized as an important morphological feature of this class of objects ($Setal07$, Sahai et al. (2011)). About half of post-AGB objects that are known (or likely) binaries show prominent disks (van Winckel 2003) (dubbed "dpAGB" objects: Sahai et al. 2011), and have very weak (or no) outflows.

The current consensus is that the primary PN formation/shaping process is hydrodynamic sculpting of the progenitor AGB mass-loss envelopes, from the inside-out by wandering and/or episodic jets during the short-lived ($\sim$1000 yr) PPN phase (Sahai & Trauger 1998; Soker 2002; Balick & Frank 2002). Support for this conclusion is provided by the fact that the momenta associated with PPN outflows, as inferred from analysis of CO observations of PPNe, either single-dish (e.g., Bujarrabal et al. (2001)) or interferometric (mostly with angular resolution poorer than $\sim 1'' - 2''$ (e.g., Cox et al. (2000); Alcolea et al. (2007); Castro-Carrizo et al. (2010); Sahai & Patel (2015); Olofsson et al. (2019)) show that these cannot be radiatively-driven. The jets are believed to result from the binary interaction; magnetic fields may play a role in PN-shaping as well, but are also most likely induced by close binaries (e.g., García-Segura et al. (2016)).

Hydrodynamic simulations of close binary interaction (e.g., leading to common-envelope evolution) have long struggled to describe even the simplest cases (e.g., Reichardt et al. (2019)), hence quantitative models that can explain the resulting jet and waist formation are lacking. An analytical approach by Blackman & Lucchini (2014) (hereafter $BL14$) predicts specific observational signatures corresponding to various possible modes of binary interaction. $BL14$ used the (limited) outflow data known for a sample of PPNe at "face-value", to derive the minimum required mass-accretion rates ($\dot{M}_a \propto M_j\,V_j/t_{acc}$), where $M_j\,V_j$ is the total jet momentum and t_{acc} is the accretion time-scale, and inferred that accretion modes such as Bondi-Hoyle-Lyttleton (BHL) wind-accretion and wind Roche lobe overflow (wRLOF) were too weak to power these

https://doi.org/10.1017/S1743921324000498 Published online by Cambridge University Press

Table 1. Target Sample: Physical Properties.

Name (IRAS)	Spec. Typ.	^{a}HST Prim. Morph.	^{b}Point Symm. *PS*	^{c}Size $('') \times ('')$	Dist. (kpc)	^{d}CO Morph., Kinematics; (FWZI[km s^{-1}])	^{e}Cont- inuum (TM1)
06530−0213	F 5Ia	M	s	0.6×1.1	1.3	Mp Ofl,W,oR; (30)	NoCen
08005−2356	F 5Ie	B	s	0.6×1.4	3	Mp Ofl; (270)	Cen
09371+1212	K 7III	M	m, an, s	?	3	?; (55)	Cen
10197−5750	A 2Iab	B	s	2.1×3.6	2	Bp Ofl,W; (100)	Cen
17047−5650	WC 10	M	m	2.6×6.2	1.35	Mp, W; (142)	Cen
17106−3046	F 5I	B	s	0.7×1.1	4	Bp Ofl; (55)	Cen($1'' \times 0.''45$)
19024+0044	G 0-5	M	m, an	1.5×2.1	3.5	Mp Ofl; (100)	NoCen
19374+2359	B 3-6	B	s	1.8×2.4	5	Mp Ofl; (375)	NoCen

Notes to Table: (a) Optical (HST) Prim. Morph.: B=Bipolar, M=Multipolar; (b) Point Symmetry: multiple pairs of lobes=$PS(m)$, ansae=$PS(an)$, shape=$PS(s)$ (details in Sahai et al. (2011)); (c) Semi-minor and semi-minor axes of smallest ellipse that includes observed CO emission (for IRAS 06530, the size refers to the inner aspherical nebula, and excludes the outer ring); (d) CO (ALMA) Prim. Morph. (from TM1 & TM2 data): Bp Ofl=bipolar outflow, Mp Ofl=Multipolar Outflows, W=waist/torus, oR=outer ring, ps=point-symmetry present, ?=unclear (most flux apparently resolved out), FWZI=full-width at zero-intensity; (e) Continuum (ALMA): NoCen=no centrally-peaked continuum source in TM1 observations, Cen=centrally-peaked continuum source [FWHM (major×minor) if resolved].

outflows. However, successful application of BL14's method needs an accurate determination of the fast outflows' physical properties in a representative morphological sample of PPNe, especially $M_j\, V_j$, and t_{acc}.

To this end, we are carrying out a systematic program of high-fidelity, $0.''1$ ALMA imaging of PPNe (*P*re-planet*A*ry *N*ebulae high-angular-res*O*lution su*R*vey with *ALMA* or PANORAMA). From our observations, we will estimate the minimum mass-accretion rate using (a) $\dot{M}_a = Q\, \sum_{k=1}^{n} M_{j,obs}\, V_{j,obs}/t_{accr(k)} = \sum_{k=1}^{n} \int\, dm(V_{off}) \times |V_{off}|\, /(sin(i_k)\, t_{accr(k)})$ (using eqns. 2 from $BL14$ and Bujarrabal et al. (2001)), where $dm(V_{off})$ is the emitting mass in a small velocity interval at an offset velocity $V_{off} = V_{lsr} - V_{sys}$, n is the number of multiple outflow-pairs, i_k is the inclination angle relative to the sky-plane and $t_{accr(k)} \lesssim t_{exp(k)}$ is the acretion time-scale for the k'th outflow-pair, and Q is a numerical factor typically satisfying $1 < Q < 5$ in jet models. For a bipolar outflow, n=1. The value of $dm(V_{off})$ is sensitive to the excitation temperature, $T_{ex}(V_{off})$, which we will estimate using the CO(6–5)/CO(3–2) ratio as a function of V_{off}.

2. The PANORAMA Survey

The PANORAMA survey covers a small (8), but representative sample of bipolar and multipolar Pre-Planetary Nebulae (PPNe), with the ultimate goal of providing quantitative constraints on the shaping mechanism(s). All objects have been previously imaged in the optical with HST, allowing a detailed classification of their morphology ($Setal07$). The survey sample includes objects that are (i) at the high end of the range of observed fast-outflow momenta ($M_j \sim 10^{39}$ g cm s^{-1}: extreme outflow object IRAS 19374) or at the low end ($M_j \sim 10^{36}$ g cm s^{-1}: IRAS 19024, Sahai et al. (2005)); (ii) with different kinds of point-symmetry, indicative of different kinds of jet activity – e.g., $PS(s)$: continuous jet with time-variable axis as in IRAS 10197; $PS(an)$: episodic jet with time-variable axis, or simultaneous multiple jets as in IRAS 19024; and (iii) with and without halos (e.g., IRAS 19374 & IRAS 17106), i.e., with high and low progenitor AGB mass-loss rates, respectively.

Survey Highlights: Although the survey, requiring observations with the 12-m array in the TM1, TM2 configurations and the 7-m array (with angular resolutions of $\sim 0.''1$, $\sim 0.''5$, $\sim 5''$, respectively) is still in progress, the existing data includes TM1 imaging of all 8 objects in one or both of Bands 7 and 9, which include the CO(3–2) and CO(6–5) lines, respectively. The results are remarkable, generally showing the presence of extended, collimated lobe-structures in CO that presumably result from bipolar or

https://doi.org/10.1017/S1743921324000498 Published online by Cambridge University Press

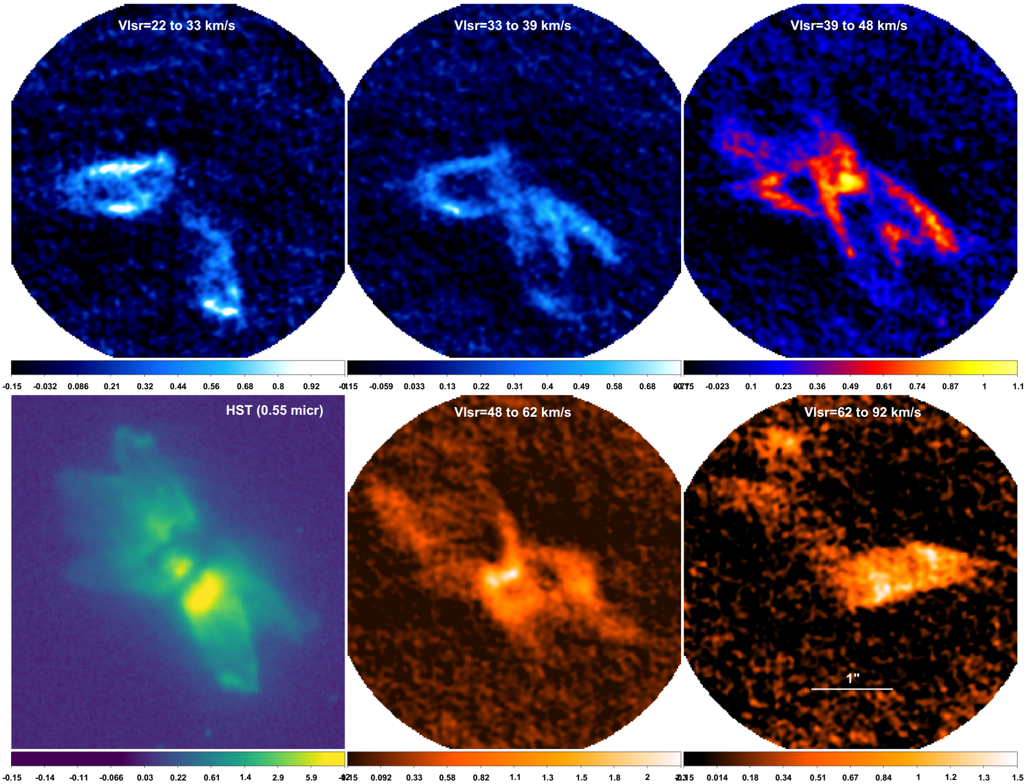

Figure 1. CO(6–5) TM1 images of IRAS 19024 in different velocity ranges within its spectrum chosen to show the shapes of its multipolar lobes for comparison with those seen in scattered light with HST in the optical. The systemic velocity is $V_{lsr} \sim 50\,\mathrm{km\ s^{-1}}$.

multipolar ($V_{exp} \sim 30\,\mathrm{km\ s^{-1}}$) outflows (Figs. 1,2). For IRAS 09371, the imaging suffers from strong artifacts that obscure its structure (Castro-Carrizo et al. 2005). The maximum (projected) outflow velocities, estimated from the spectra, can be broadly classified into 3 classes: extreme (i.e., $V_{exp} \gtrsim 70\,\mathrm{km\ s^{-1}}$: IRAS 17047 and IRAS 19374), medium ($70 > V_{exp} > 30\,\mathrm{km\ s^{-1}}$: IRAS 09371, IRAS 10197, IRAS 17106, and IRAS 19024) and low (IRAS 06530: we discuss this object in detail below). Three optically-classified bipolar objects show the possible presence of an additional (fainter) outflow with a different orientation than the optical symmetry axis, indicating that these objects may also be intrinsically multipolar.

The high angular-resolution maps enable us to isolate the dense waists from the low-latitude region of the outflows in the target sample and resolve their true structure. One of the surprising results is the conspicuous absence of gas close to the central star in the majority of objects, suggesting that the waist structures have a toroidal structure, resulting from an episode of equatorially-enhanced mass-loss from the progenitor AGB, as for e.g., in a CE system (e.g., Sandquist et al. (1998); Passy et al. (2012)). This result is in marked contrast to dpAGB objects, such as the Red Rectangle, AC Her, and IW Car (Bujarrabal et al. 2013, 2015, 2017), that show compact rotating disks of gas+dust, with masses of $\sim 0.0012 - 0.006\,M_\odot$; these may have formed due to enhanced RLOF ($BL14$).

Continuum emission was detected towards all sources in the existing data, which can be divided into 3 broad classes, using the TM1 images (i) extended emission + unresolved central source, (ii) extended central source, (iii) extended emission and no central source

https://doi.org/10.1017/S1743921324000498 Published online by Cambridge University Press

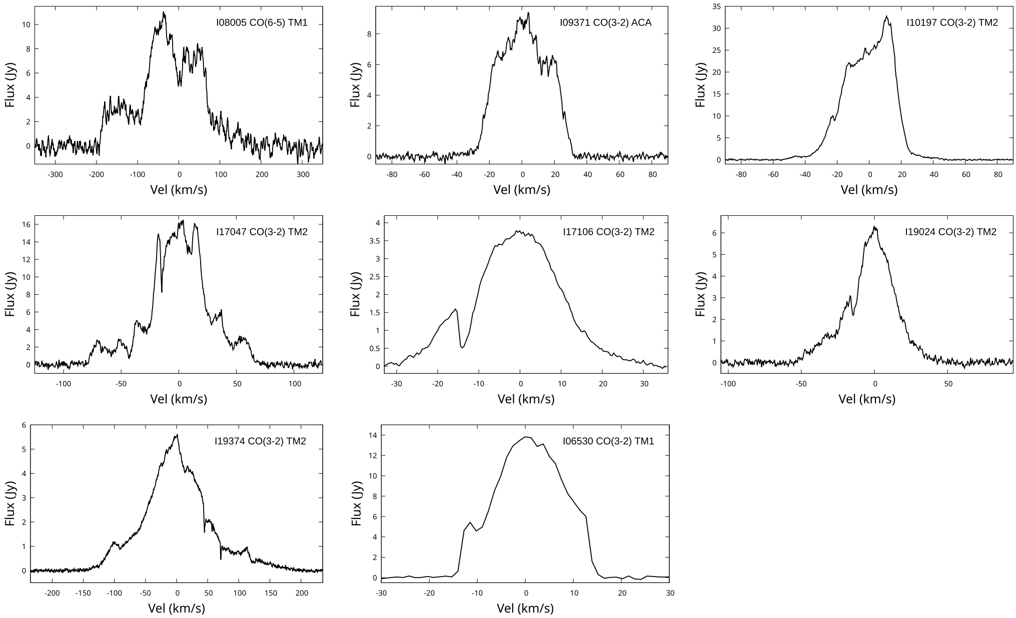

Figure 2. Representative (spatially-integrated) CO J=6-5 or 3-2 spectra, for the PANORAMA sample of PPNe. The systemic velocity has been set to zero for each object.

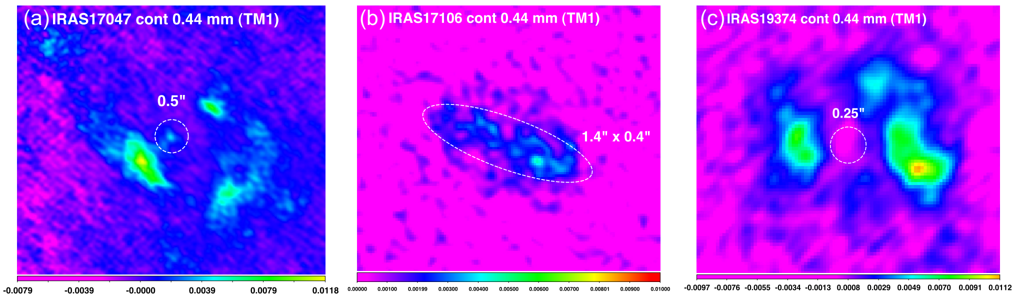

Figure 3. Three classes of continuum emission (0.44 mm TM1 data) (a) extended emission + compact central source, (b) extended central source, (c) extended emission, no central source. The dashed circles or ellipse (with sizes) show the location of the central star.

(e.g., Fig. 3). These data emphasize the importance of high-resolution observations to characterize the origin and nature of the (sub)mm emission, since lower-reolution studies, with angular resolution $\gtrsim 0\farcs5$ would tend to merge the compact and extened emission into one structure, which could then be mis-interptreted as being a dpAGB-type disk, for example.

IRAS 06530: IRAS 06530 shows a large geometrically-thin ring, surrounding a compact central nebula that has a high degree of point-symmetry (Table 1). Unlike the other PPNe in our sample, no high-velocity emission is seen – the value of V_{exp} ($\lesssim 12.5$ km s^{-1}) is similar to what is typically found for outflows during the AGB phase. Such rings have been seen in several carbon stars and attributed to an episodic increase in the mass-loss rate due to a thermal pulse. Thus, the ring in IRAS 06530 is due to the last thermal pulse while its central star was still on the AGB. Following the thermal pulse, there was a steep decrease in the mass-loss rate (by a factor $\gtrsim 10$) for ~ 600 yr. During this latter period, the mass loss was not spherically symmetric (Fig. 4a). It was then followed by a new episode

https://doi.org/10.1017/S1743921324000498 Published online by Cambridge University Press

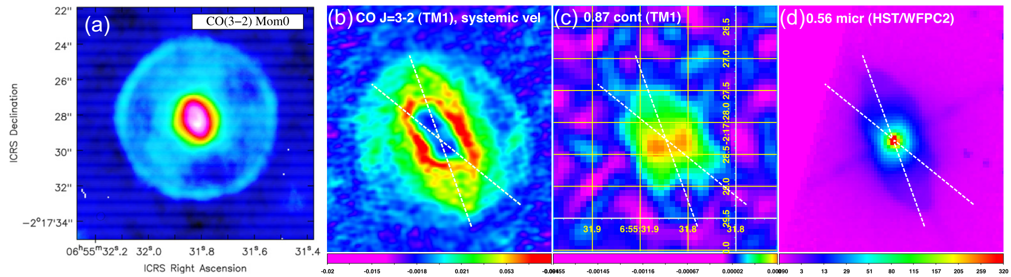

Figure 4. The multipolar PPN IRAS 06530: (a) Moment 0 map of the CO(3–2) (TM2), (b) Map of CO(3–2) at the systemic velocity showing the structure of the central bipolar nebula (TM1), (c) 0.89 mm TM1 continuum image, (d) HST/WFPC2 0.56 μm image of scattered light. The dashed lines show the axes of two pairs of lobes seen in the optical. Panels $b - d$ have the same field-of-view.

of enhanced mass loss immediately preceding the start of the CS's post-AGB evolution; the resulting shell shows extended arc-like structures that are likely part of a 3-D spiral structure resulting from interaction with a companion (such spiral structures are being found in a growing list of AGB stars, see e.g. Decin et al. (2020)). From the expansion ages of the ring (5500 yr) and waist (750 yr), we infer that IRAS 06530 transitioned from an AGB star to a post-AGB star 4750 yr ago. A full description and analysis of these data will be presented in a forthcoming paper (Sahai et al. (2024)).

In summary, the PANORAMA survey has produced several exciting results and some unexpected ones as well. The morphology of the molecular gas, in almost all cases shows the presence of collimated outflows that correspond to the lobes seen in optical scattered light, confirming that the latter result from sculpting of the ambient circumstellar envelope (ejected by the prognenitor AGB star). But there is one notable exception, the C-rich PPN IRAS 06530, which shows an extended ring due to the last thermal pulse. In a few optically-bipolar objects, additional faint outflows misaligned with the symmetry axis are found, indicating that these objects may be multipolar. Compact continuum emission around the central star is seen in some sources, but not in others – in contrast to dpAGB objects, where such emission is one of their defining characteristics.

Acknowledgements

RS's contribution to the research described here was carried out at the Jet Propulsion Laboratory, California Institute of Technology, under a contract with NASA, and funded in part by NASA via ADAP awards, and multiple HST GO awards from the Space Telescope Science Institute.

References

Alcolea et al. 2007, *A & A*, 468, L41
Balick, B. & Frank, A. 2002, *ARA & A*, 40, 439
Balick et al. 2020, ApJ, 889, 13
Blackman & Lucchini 2014, MNRAS, 440, L16 (*BL*14)
Bond, H. E., Henden, A., Levay, Z. G., et al. 2003, *Nature*, 422, 405
Bujarrabal, V., Castro-Carrizo, A., Alcolea, J., et al. 2001, *A & A*, 377, 868
Bujarrabal, V., Castro-Carrizo, A., Alcolea, J., et al. 2013, *A & A*, 557, L11
Bujarrabal, V., Castro-Carrizo, A., Alcolea, J., et al. 2015, *A & A*, 575, L7
Bujarrabal, V., Castro-Carrizo, A., Alcolea, J., et al. 2017, *A & A*, 597, L5
Castro-Carrizo, A., Bujarrabal, V., Sánchez Contreras, C., et al. 2005, *A & A*, 431, 979
Castro-Carrizo, A., Quintana-Lacaci, G., Neri, R., et al. 2010, *A & A*, 523, A59
Cox, P., Lucas, R., Huggins, P. J., et al. 2000, *A & A*, 353, L25

https://doi.org/10.1017/S1743921324000498 Published online by Cambridge University Press

Decin, L., Montargès, M., Richards, A. M. S., et al. 2020, Science, 369, 1497
De Marco, O. & Izzard, R. G. 2017, *Publ. Astr.. Soc. of Australia*, 34, e001
García-Segura, G., Villaver, E., Manchado, A., et al. 2016, *ApJ*, 823, 142
Ivanova, N., Justham, S., Chen, X., et al. 2013, A&ARv, 21, 59
Lagadec, E., Verhoelst, T., Mékarnia, D., et al. 2011, *MNRAS*, 417, 32
Olofsson, H., Khouri, T., Maercker, M., et al. 2019, *A & A*, 623, A153
Passy, J.-C., De Marco, O., Fryer, C. L., et al. 2012, *ApJ*, 744, 52
Reichardt, T. A., De Marco, O., Iaconi, R., et al. 2019, *MNRAS*, 484, 631
Sahai, R. & Patel, N. A. 2015, *ApJ Let*, 810, L8
Sahai, R. & Trauger, J. T. 1998, *AJ*, 116, 1357
Sahai, R. and the PANORAMA consortium, 2024, ApJ (in prep.)
Sahai, R., Sánchez Contreras, C., & Morris, M. 2005, *ApJ*, 620, 948
Sahai, R., Morris, M., Sánchez Contreras, C., et al. 2007, *AJ*, 134, 2200
Sahai, R., Morris, M. R., & Villar, G. G. 2011, *AJ*, 141, 134
Sahai, R., Claussen, M. J., Schnee, S., et al. 2011, *ApJ Let*, 739, L3
Sandquist, E. L., Taam, R. E., Chen, X., et al. 1998, *ApJ*, 500, 909
Siódmiak, N., Meixner, M., Ueta, T., et al. 2008, *ApJ*, 677, 382
Soker, N. 2002, *ApJ*, 568, 726. doi:10.1086/339065
Stanghellini, L., Shaw, R. A., & Villaver, E. 2016, *ApJ*, 830, 33
Tocknell et al. 2014, *MNRAS*, 439, 2014
Tylenda, R., Hajduk, M., Kamiński, T., et al. 2011, *A & A*, 528, A114
Ueta et al. 2000, ApJ, 528, 861
van Winckel, H. 2003, *ARA & A*, 41, 391
Zou, Y. et al. 2020, MNRAS, 497, 2855